Characterization of GaSb/Sb Heterostructures By Scanning Tunneling Microscopy

Chad Sosolik

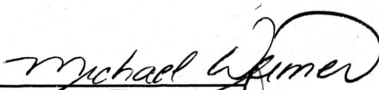University Undergraduate Research Fellow, 1994-95

Texas A&M University
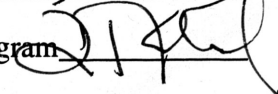
Department of Physics

APPROVED

Undergraduate Advisor _Michael Weimer_

Exec. Dir., Honors Program

CHAPTER 1

Introduction

Background

Since its invention in 1982 by Binnig and Rohrer [1], the scanning tunneling microscope (STM) has become an invaluable tool in the characterization of materials. With its ability to image features down to the atomic level and to probe electronic structure, the STM can thoroughly characterize a material's surface. With new artificially structured materials being fabricated by various epitaxial methods, researchers have a wealth of new surfaces to explore with the STM.

Before discussing any of these materials, one must have a grasp of the physics behind scanning tunneling microscopy. The STM utilizes the quantum mechanical phenomenon of tunneling. Tunneling in the STM involves the transmission of an electron through a potential barrier which, considering its kinetic energy, it could not surmount according to classical mechanics. This effect is due to the wave properties possessed by the electron. However, tunneling is not unique to matter waves and can be illustrated on a larger scale using total internal reflection of light in a prism.

In this example of optical tunneling, light is incident on a glass-to-air surface at the back face of a prism. At an angle greater than the critical angle, total internal reflection occurs, and no light is transmitted. However, because light is a wave, the electric field does not go to zero at the glass-to-air surface. Instead, it decreases exponentially to a negligible value within a few centimeters of the surface. Thus, when a second prism is brought near the surface, light is transmitted through it. The light has "tunneled" across the barrier of air. This air barrier, the "forbidden region" where no traveling wave solution to Maxwell's wave equation exists, serves the same role as the potential barrier experienced by an electron outside a solid. The wave nature of the electron requires that it obey the Schrodinger equation, so just as light penetrated the air barrier and was transmitted, so can the electron, as a wave, penetrate a potential barrier and be transmitted [2,3]. The potential barrier is a "forbidden region" for the electron, where no traveling

wave solution to the Schrodinger equation exists. A key difference between the prism example and electron tunneling is that the exponential decrease of the electron wave function occurs over a much smaller length scale. Instead of decreasing within a few centimeters (1cm = 10^{-2} m) as the light does, the electron wave function becomes negligible within a few angstroms (1Å = 10^{-10} m).

The STM uses tunneling by the electron to image surfaces and to measure other important properties of materials. In the STM, a sharp conducting tip is brought near the surface of the sample to be studied. The vacuum region between the tip and the surface serves as the potential barrier. This barrier can be represented in a graph of energy versus position (E vs. x). Figure 1 shows a series of E vs. x graphs for an STM tip and sample. The topmost graph illustrates the potential barrier of the vacuum between the separated tip and sample. Neglecting thermal excitation, the Fermi levels, E_F, denote the dividing line between filled and unfilled electron states. They differ by an amount equal to the work function difference. The work function, Φ, is the minimum energy required to remove an electron from the bulk to the vacuum level. When the tip and sample are brought into electrical contact and equilibrium is achieved, there is one unique Fermi level as illustrated in the middle graph of Figure 1. The bottom graph of Figure 1 represents E vs. x as the tip and sample are brought closer together, and a voltage V is applied between them to influence tunneling in one direction and to obtain a net tunneling current. The Fermi levels now differ by an amount eV. The arrows show the energy range over which tunneling may occur. At higher energies, there are no electrons to tunnel, while at lower energies, by Pauli exclusion, there are no empty states to tunnel into [4]. Thus, if one brings the tip and sample into equilibrium and measures the tunneling current while varying the bias voltage, a graph of current versus voltage can be obtained, as illustrated in Figure 2. This figure helps illustrate a key difference between a metal and semiconductor sample. An energy gap, E_g, exists in a semiconductor. It is this gap which is responsible for the versatile electronic properties of semiconductors. Tunneling cannot occur in this energy range, and therefore, the tunnel current is zero, as shown in the figure. With such data one may determine the width of the energy gap and the location of the sample Fermi

level, E_F, within the gap, which are both important for understanding the sample's electronic properties.

The STM is also used to obtain surface images with a resolution comparable to the size of an atom. This high degree of resolution is obtainable because of the small length scale involved in electron tunneling. Minute changes in tip-surface separation result in detectable variations in tunneling current. For example, an increase of only 0.01 angstrom in tip-surface separation will result in a 2% decrease in tunneling current. In obtaining an image, the conducting tip is again brought near the surface and a bias voltage applied. The position of the tip in three dimensions is controlled by piezoelectric drivers. Using these drivers, the tip is scanned in the two lateral dimensions while the tip height is adjusted to keep the tunneling current constant. Plotting the tip height versus the two lateral dimensions yields an image of the surface [5].

The images one obtains are dependent on the applied bias voltage. In a typical semiconductor electrons will tunnel *out* of the *valence* band and *into* the *conduction* band. Therefore, the images obtained for such a semiconductor will reflect the spatial distribution of the valence and conduction band wave functions. For example, in GaSb, the conduction states are mainly localized on the Ga atoms, while the valence states are localized on the Sb atoms. Therefore, with either a positive or negative sample bias, one achieves atom-selective imaging of either Ga or As atoms, respectively [6].

Artificially Structured Materials

Before discussing in any detail the specific structures to be studied with the STM, one must qualitatively understand the meaning of some terms. Specifically, these terms are *ternary alloy*, *heterostructure*, and *superlattice*. Each of these will be defined in the context of an example specific to semiconductor physics.

Ternary alloys, as the name suggests, are composed of three elements. For example, $Al_xGa_{1-x}N$ is considered a ternary alloy. The material $Al_xGa_{1-x}N$ is essentially GaN with a fraction x of the Ga lattice positions being occupied by Al atoms. For instance, if x=0.25, then

there are 25% Al atoms and 75% Ga atoms. The placement of Al atoms on Ga lattice sites is random. By substituting the Al for Ga, one has changed the bulk properties of the material. Of interest here is the ability to controllably alter the value of the band gap by varying x. For example, the band gap of $Al_xGa_{1-x}N$ can be "tuned" from 3.4 to 6.2 eV [7]. This "tunability" of the band gap allows one to create materials with a specific gap value that is useful for a particular application.

Heterostructures involve an interface between two materials. Examples include the metal-semiconductor interfaces in Schottky barriers (e.g. Au/Si) and the semiconductor-semiconductor interfaces in quantum well structures (e.g. GaAs/AlAs). More recently, semiconductor-semimetal interfaces (e.g. GaSb/Sb) have also been fabricated. Unlike the ternary alloys, the bulk properties of the materials comprising a heterostructure are not changed. Instead, the properties change abruptly at the interface.

An interesting new material results when these layers are grown on top of one another. For instance, if the GaAs/AlGaAs heterostructure is periodically repeated so that there are alternating layers of GaAs, AlGaAs, GaAs, etc., then one has created a *superlattice*. Another example is the GaSb/Sb superlattice which consists of alternating layers of GaSb and Sb. The superlattice is differentiated from the previous ternary alloy structure by the fact that the arrangements of its constituents are periodic on the order of 10-100 angstroms, whereas the addition of Al "impurities" to the $Al_xGa_{1-x}N$ described above resulted in the integration of the Al atoms into a GaN lattice at random locations [8]. One should note that if the repeated layers in the superlattice are thin, the properties within each layer will differ from those of the bulk.

Experiment

GaSb/Sb heterostructures hold the promise of being very interesting materials. Properties introduced by the growth of the semiconductor and semi-metal together may prove to be very useful in various electronic devices [9]. Various configurations of were grown at the University of Houston for STM characterization. The equipment necessary for the characterization of the

heterostructures was already in place in the laboratory. Using this equipment, samples were placed in an ultra-high vacuum(UHV) system by means of a linear motion device. They were cleaved in UHV to expose a clean surface and then transported by means of a second linear motion device to the STM. There a characterization using of their electronic and spatial structure was made. Specifically, band gap values and offsets were determined, as well as Fermi levels. Also, with the imaging capabilities of the STM, the surface structure was investigated. Special tips were fabricated for this work.

REFERENCES

[1]   G. Binnig and H. Rohrer, Helvetica Physics Acta **55**, 726 (1982).

[2]   A. Sommerfeld, *OPTICS* (Academic Press, New York, 1964).

[3]   P. Tipler, *Modern Physics* (Worth Publishers, Inc., New York, 1992).

[4]   J.A. Stroscio and W.J. Kaiser, *Scanning Tunneling Microscopy* Methods of Experimental Physics (Academic Press, New York, 1993), vol. 27.

[5]   R.A. Serway, C.J. Moses, and C.A. Moyer, *Modern Physics* (Harcourt Brace Jovanovich College Publishers, New York, 1989).

[6]   J.A. Stroscio, R.M. Feenstra, and A.P. Fein, Phys. Rev. Lett. **58**, 1558 (1987).

[7]   M.A. Khan, A.R.B. Kuzznia, and D.T. Olson, Appl. Phys. Lett. **62**, 1786 (1993).

[8]   F. Capasso and G. Margaritondo, *Heterojunction Band Discontinuities: Physics and Device Applications* (Elsevier Scientific Publications, North Holland, 1989).

[9]   J.A. Dura, A. Vigliante, T.D. Golding, and S.C. Moss, J. Appl. Phys. **77**, 21 (1995).
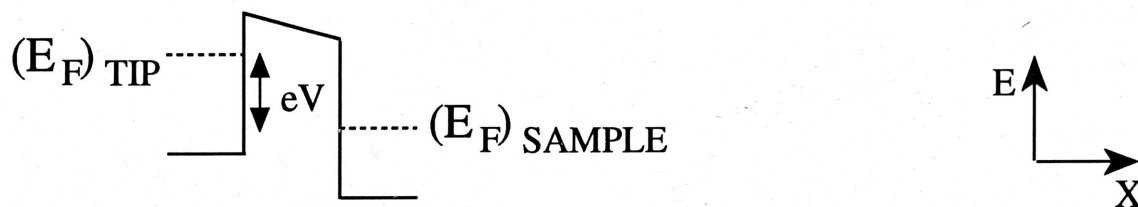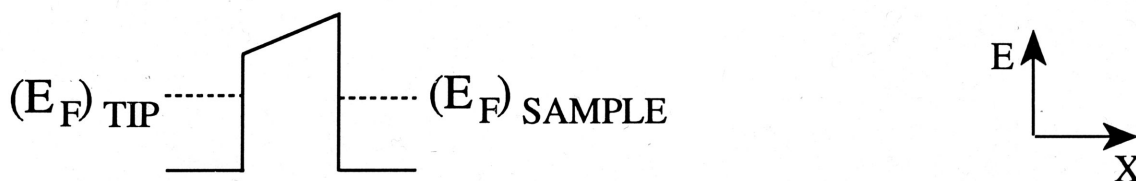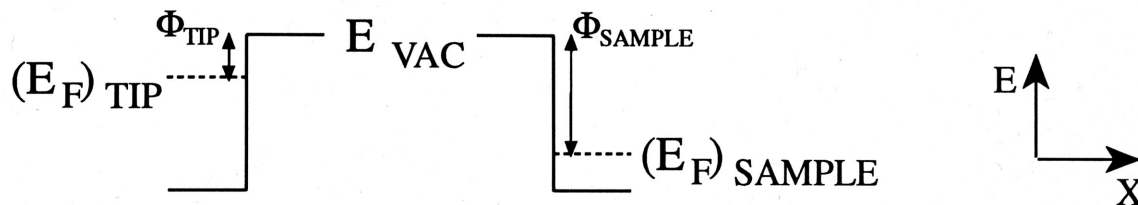
Figure 1

Band Diagrams of the Tunneling Junction
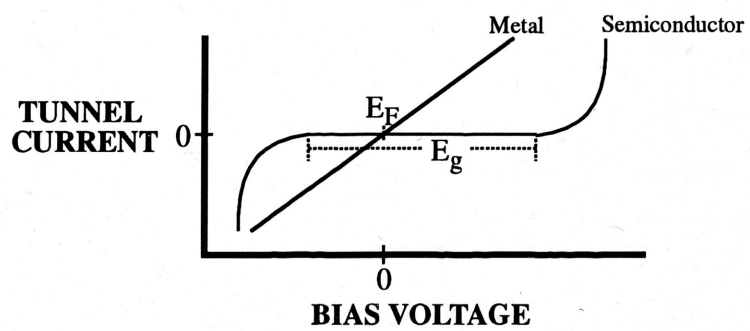
Figure 2

Schematic of Current V.s. Voltage

CHAPTER 2

Tip Fabrication

The tip plays an integral role in the ability of the STM to image surfaces at the atomic level. The resolution of the microscope is directly tied to the geometry of the tip. For samples with very little topography, the range of usable tip shapes is rather wide, since tunneling will occur across the smallest gap between the tip and sample. However, as the sample surface morphology becomes more varied, the tip geometry becomes very important, placing limits on the range of usable tip shapes.

Motivation

In order to examine heterostructures with the STM, the epitaxially grown superlattice layers must first be found, and this requires moving to the edge of the sample as shown in Figure 1. It is this edge-finding requirement that brings the tip geometry to the forefront. The first step in the edge-finding process involves bringing the tip within approximately 30 microns of the edge. During this step, the operator controls the tip's motion across the surface while observing the tip and sample through the stereoscopic microscope mounted above the STM. The microscope is a Nikon SMZ-2B and has a resolution of 30 microns. Next, the tip is moved repetitively in steps of 30,000 Å across the sample surface toward the edge. After each movement, the tip is brought in toward the surface until tunneling occurs. By noting the z-piezo readouts after each movement, it can be determined how far the tip had to extend before tunneling occurred. This gives a measure of the relative heights of areas on the sample surface. Eventually the tip is observed, by means of the z-piezo readout, to "dive in" towards the sample. This is the point where the tip has moved off of the surface and tunneling now occurs out of some point on the side of the tip. To further localize the sample edge, the tip is retracted and the distances of movement on and off the edge are repeatedly halved until it is certain that the tip is precisely over the edge. It is here that the tip geometry comes into play. As noted earlier, tunneling between the tip and sample occurs across

the shortest tip sample distance. Therefore, if the end of the tip is blunt or rounded, tunneling could occur over an extended range out of one area on the sample while the tip continues to move. This will result in a distortion of the edge image by a convolution of the tip geometry into the image as well as significant error in the localization of the position of the edge, as illustrated schematically in Figure 2. This problem will be less severe if the tip is sharp. Therefore, our first task was to fabricate reproducibly sharp STM tips.

Basic Techniques

Various methods are employed in the fabrication of STM tips, the most common being mechanical shearing and electrochemical etching. Mechanical shearing simply involves the cutting or grinding of a metal wire. The geometry produced in the shearing process is quite random, producing some blunt-ended and asymmetric tips. Tips with this type of geometry are useful on atomically flat surfaces where the overall structure of the tip is unimportant and the small protrusions on the end can serve as mini tips. However, this type of tip raises concerns about reproducibility, lack of symmetry, low aspect ratio, and the possibility of multiple tips on surfaces that are not atomically flat. Tip shapes that are symmetric and reproducible can be produced by electrochemical etching. Electrochemical etching comes in many forms, but there is a basic procedure which is common to all etching. The procedure consists of the immersion of a metal wire into an appropriate electrolyte with an applied AC or DC voltage. The wire is etched against an appropriate form of counter-electrode. As material is etched away, the meniscus formed around the immersed wire slowly descends creating a tapered shape. The increased rate of etching taking place along the wire-liquid-air junction eventually cuts the wire removing the immersed portion and leaving a sharp, tapered metallic tip at the liquid-wire interface. The sharpness of an etched tip can be refined through electropolishing techniques borrowed from field ion microscopy. One specific technique, which was employed here, is akin to zone electropolishing [1] where the very end of the tip is immersed in a thin film of etchant solution suspended in a small wire loop at a low voltage.

The tip can be moved in and out of the film of solution for thinning, or the very end of the tip can be brought into contact with the film for sharpening.

Materials

Various materials have been used as tips for the STM. The three most commonly used in the STM laboratory at Texas A&M are tungsten (W), platinum (Pt), and platinum/iridium (Pt/Ir).

Tungsten is a common material chosen for STM tips because it is stiff and can be etched to produce very sharp tips. Fotino [2] has reported success with a two step AC etching procedure in which tungsten is etched in a normal downward position and is then re-etched for sharpening in a reversed position. Ibe *et al.* [3] have shown success using a DC etching procedure which can produce tips with radii of curvature down to 20 nm. This method is similar to a DC etch procedure used in the STM laboratory which produces tips like that seen in Figure 3. One drawback to using tungsten, which neither method addresses, is the fact that tungsten develops a thick electrochemical oxide layer which must be removed before it can be used for effective imaging. Various methods devised to remove the oxide layer include field emission [4], sputtering [5], ion milling [6], and electron bombardment [7]. A simple oxide removal method demonstrated by Hockett *et al.* [8] consists of the immersion of the tungsten in hydrofluoric acid. This method has been used recently with some success in our laboratory.

Pt and Pt/Ir tips are inert to oxidation and for this reason are often chosen over tungsten tips. Mechanically sheared or "cut" Pt tips have been used extensively in the STM lab with success on various atomically flat samples. An example of this type of tip can be seen in Figure 4. The addition of Ir to form a Pt/Ir alloy is preferable since the Ir adds stiffness to the Pt, which is an otherwise softer metal than W. Musselman *et al.* [9] have shown how Pt/Ir can be electrochemically etched to form sharp tips with geometries that are well-suited to the imaging of jagged and irregular surfaces. Their method consisted of an AC etch and re-etch in a solution of $CaCl_2/H_2O/HCl$. Pt/Ir tips have also been etched in various other solutions, including $KCl/H_2O/HCl$ [10],$NaCN/KOH$ [11], and molten $NaNO_3/NaCl$ [9].

Experimental Methods and Results

It was determined that tips appropriate for work with heterostructures could best be fabricated by following the lead of Musselman et al. [9] and electrochemically etching Pt/Ir. The material appeared an obvious choice since it required no oxide removal procedure. Also, Pt/Ir was a material not previously used in the STM laboratory, so these would be the first experiments ever carried out on the material. The tip fabrication experiments were carried out using 0.2 mm Pt/Ir 80:20 [12].

The Pt/Ir was etched in the apparatus shown in Figure 5. The etching setup consisted of a tip holder mounted above a beaker containing the etchant solution. The beaker was placed on a composite rubber pad [13] for vibration isolation. The tip was clamped in a slot in the bottom of the holder, and the entire tip/holder apparatus could be raised or lowered by means of a micrometer. The tip holder and the sheath on the wires connecting the tip and counter-electrode to the power supply were made of Teflon to reduce corrosion and possible contamination of the etchant solution. The counter-electrode was a 7 cm piece of carbon cut from a 1.27 cm diameter rod [14]. During etching, a Nikon stereoscopic microscope with a magnification range of 7x to 30x and a fiber optic lighting system could be moved into place to observe the process more closely.

In bulk etching approximately 1.5 cm of 0.2 mm Pt/Ir wire was placed in the tip holder and held at 25 VAC against the carbon counter-electrode. The wire was then immersed approximately 1.5 mm into 50 ml of saturated $CaCl_2/H_2O/HCl$ (60%/36%/4% by volume) [15]. The etching process was self-terminating upon drop-off of the lower portion of the wire, and, depending on the age of the solution, took about 5-7 minutes to complete. The variation in etching time is attributable to a depletion of the chloride ion concentration with the formation of a platinum chloride complex [16].

The re-etching procedure was performed in the same tip/holder configuration; however, the beaker and counter-electrode were replaced by a small gold loop approximately 2 mm in diameter, also illustrated in Figure 5. A thin film of etchant was suspended in the loop, and 3 VAC was

applied between the tip and loop. While watching the tip and loop through the microscope, the tip was lowered until the very end made brief contact with the film of solution.

Characterization of the Pt/Ir tips was performed by observations with a Wolfe optical microscope in the STM laboratory and with the Environmental Scanning Electron Microscope (Electroscan ESEM E-3) at the Texas A&M Electron Microscopy Center. The optical microscope had a magnification of 100x. The ESEM had a magnification range of 100x to 100,000x and a resolution of 5 nm. The ESEM was chosen over the other instruments available at the Microscopy Center because it provided the ability to study oxides on the tips and because images obtained from the instrument were in a digital format so they could be easily transferred to the STM lab for subsequent analysis.

Following each etch and re-etch procedure the fabricated Pt/Ir tip was observed under the optical microscope. This allowed for the removal of any tips which had obvious deformities, such as being blunt or bent, and it also allowed for the correlation of optical observations with the later higher resolution ESEM images. It was discovered that certain tip characteristics, both favorable and unfavorable, could be determined optically. For example, "knob-ended" tips like that seen in Figure 6 appeared to have a very bright point on their ends under the optical microscope. Sharp tips, on the other hand, had ends that were often too thin to even be observable.

The first problem encountered in etching the Pt/Ir was an asymmetry in an otherwise fairly sharp tip shape similar to that seen in Figure 7. It was first proposed that the orientation of the counter-electrode relative to the tip was a factor. However, after several orientations were investigated it was determined that the amount of etching occurring had no dependence on the counter-electrode's position. This verified previous work by Ahlers *et al.* [16]. The asymmetry was finally attributed to the angle at which the Pt/Ir wire was entering the etchant solution. To allow for a more precise determination of the tip's entry angle, the microscope and fiber optic lighting were utilized, and once it was ensured that the tip entered the solution normal to the surface, the asymmetry was eliminated.

Another problem encountered was that, after etching, the tips occasionally had shanks which were over-thinned and thus bent very easily. This was finally attributed to operator-induced vibration of the table on which the etching was taking place. This vibration was causing the etchant solution to move up the shank of the tip and etch away more material leaving a thinner shank than was desired. To eliminate this vibration, the apparatus was isolated so that once etching had begun it was unnecessary for the operator to intervene and induce any vibration. With this change in place, the over-thinning was no longer a problem. Successfully bulk etched tips appeared similar to the one shown in Figure 8.

Re-etching was initially carried out using the methods suggested by Musselman *et al.* [9]. The first re-etch step was used to thin the end of the tip by moving it through the film of etchant suspended in the gold loop. The second step involved sharpening of the tip by making only brief contact with the film. The re-etch produced much sharper tips with higher aspect ratios similar to the tip seen in Figure 9. After some experience with the re-etching procedure, it became obvious that the degree of re-etching needed was dependent on how well the bulk-etching had been done. For example, on some tips the thinning portion of the re-etch resulted in over-thinned tips that bent easily. Therefore, it was determined that the brief contact sharpening procedure be carried out on all tips while the thinning step was retained only for those tips that needed it. One use found for the thinning procedure was the ability to save the "knob-ended" tips mentioned earlier. If it was obvious that a tip had this distinctive shape, it was possible to remove it by repeated passes through the thin film of etchant. Eventually the end would fall off leaving a sharper point that could then be polished. Variations of this procedure were also successful in removing other unwanted tip shapes.

REFERENCES

[1]   A.J. Melmed and J.J. Carroll, J. Vac. Sci. Technol. A **2**, 1388 (1984).

[2]   M. Fotino, Rev. Sci. Instrum. **64**, 159 (1993).

[3]   J.P. Ibe, P.P. Bey Jr., S.L. Brandow, R.A. Brizzolara, N.A. Burnham, D.P. DiLella, K.P. Lee, C.R.K. Marrian, and R.J. Colton, J. Vac. Sci. Technol. A **8**, 3570 (1990).

[4]   V.T. Binh, Journal of Microscopy **152**, 355 (1988).

[5]   C. Schonenberger, A.F. Alvarado, and C. Ortiz, J. Appl. Phys. **66**, 4258 (1989).

[6]   D.K. Biegelsen, F.A. Ponce, J.C. Tramontana, and S.M. Koch, Appl. Phys. Lett. **50**, 696 (1987).

[7]   J.A. Stroscio, R.M. Feenstra, and A.P. Fein, Phys. Rev. Lett. **58**, 1558 (1987).

[8]   L.A. Hockett and S.E. Creager, Rev. Sci. Instrum. **64**, 263 (1993).

[9]   I.H. Musselman and P.E. Russell, J. Vac. Sci. Technol. A **8**, 3558 (1990).

[10]   E.W. Muller and T.T. Tsong, *Field Ion Microscopy, Principles and Applications* (Elsevier, New York, 1969).

[11]   M.J. Heben, M.M. Dovek, L.N. S., R.M. Penner, and C.F. Quate, Journal of Microscopy **152**, 651 (1988).

[12]   Ted Pella Incorporated, Redding, CA

[13]   E-A-R Specialty Composites, Indianapolis, IN

[14]   Alfa Aesar, Ward Hill, MA

[15]   Spectrum Chemical Manufacturing, Gardena, CA

[16]   C.T.J. Ahlers and R.W. Balluffi, J. Appl. Phys. **38**, 910 (1967).

Sample

[110]

[$\bar{1}1\bar{1}$]A

Growth Direction

Tip

Superlattice

60Å Sb
20Å GaSb
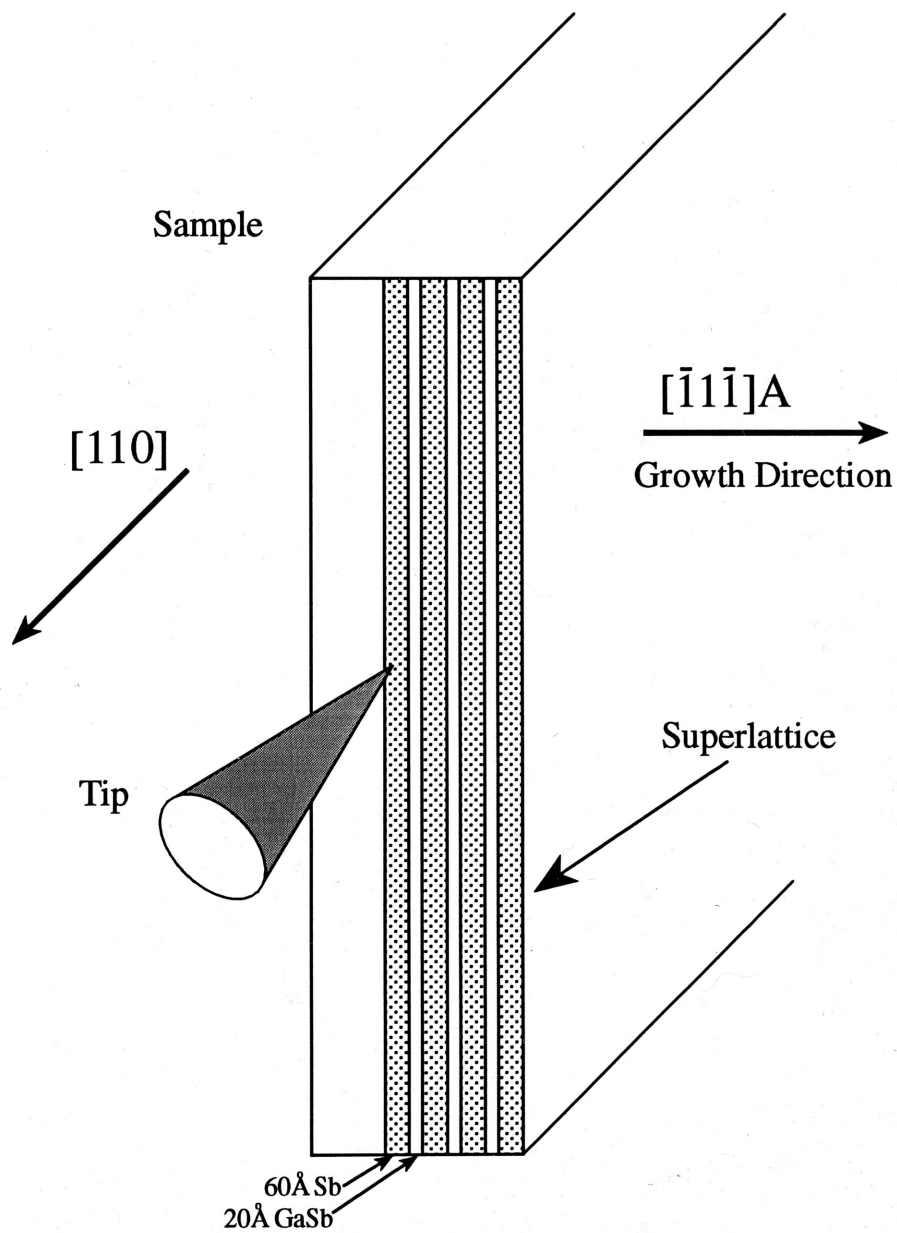
Figure 1
Cross-Sectional Scanning Tunneling Microscopy
of a Cleaved Superlattice Sample
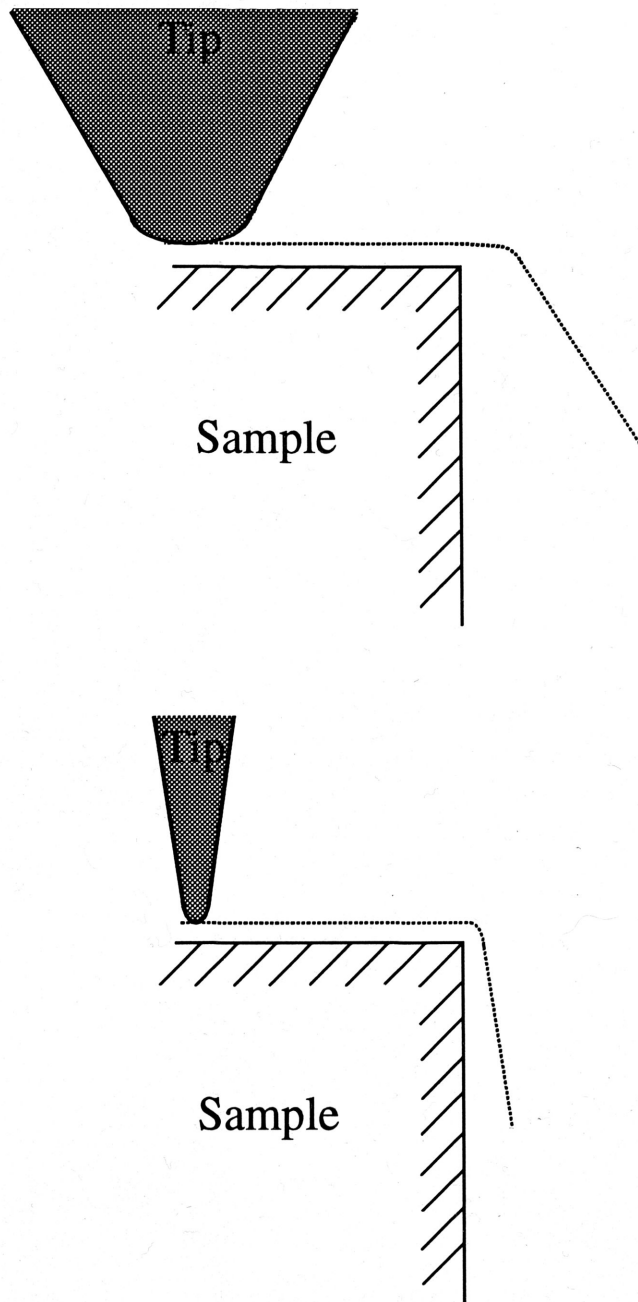
Figure 2
Effect of tip geometry on edge imaging.
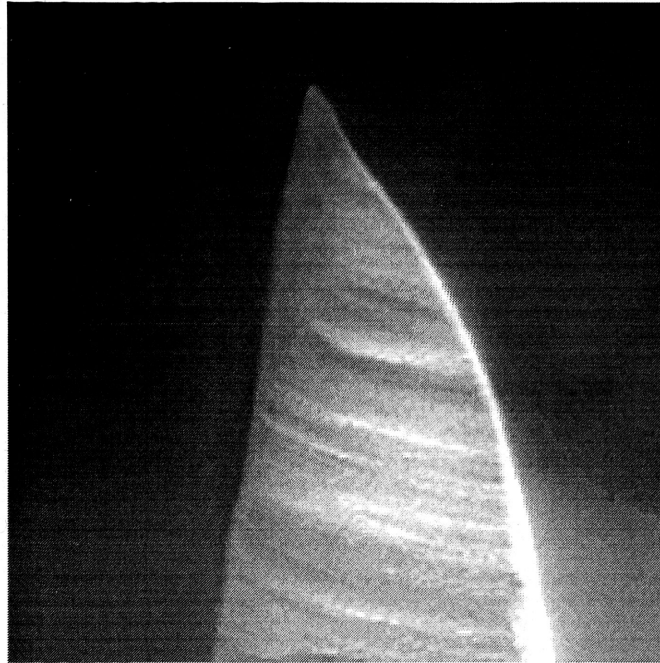Dotted lines denote STM profile traced out by tip.
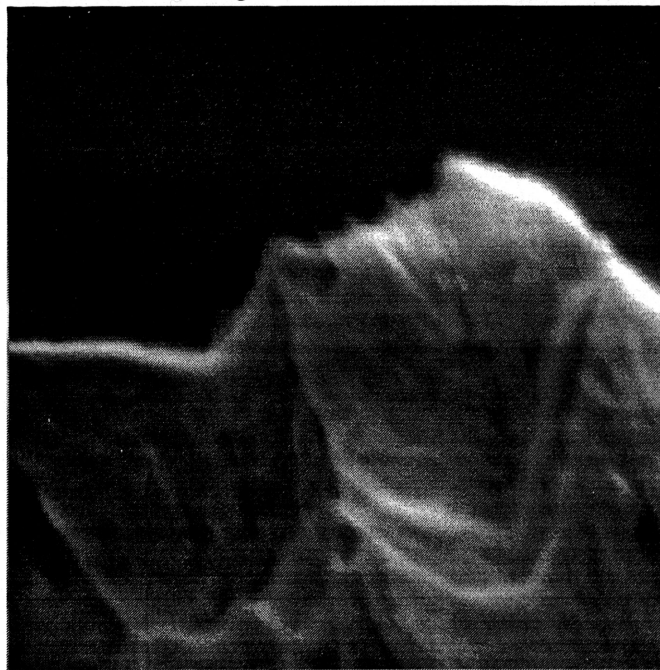
Magnification: x175
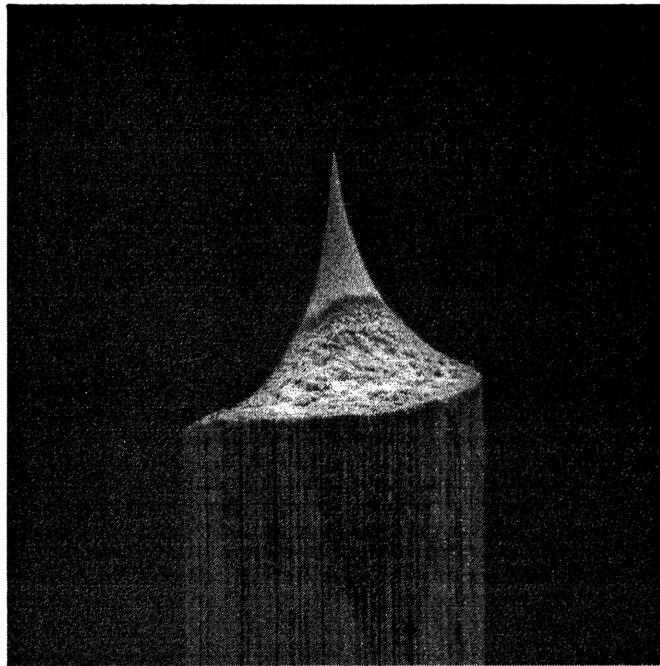
———— 100 microns

Figure 3
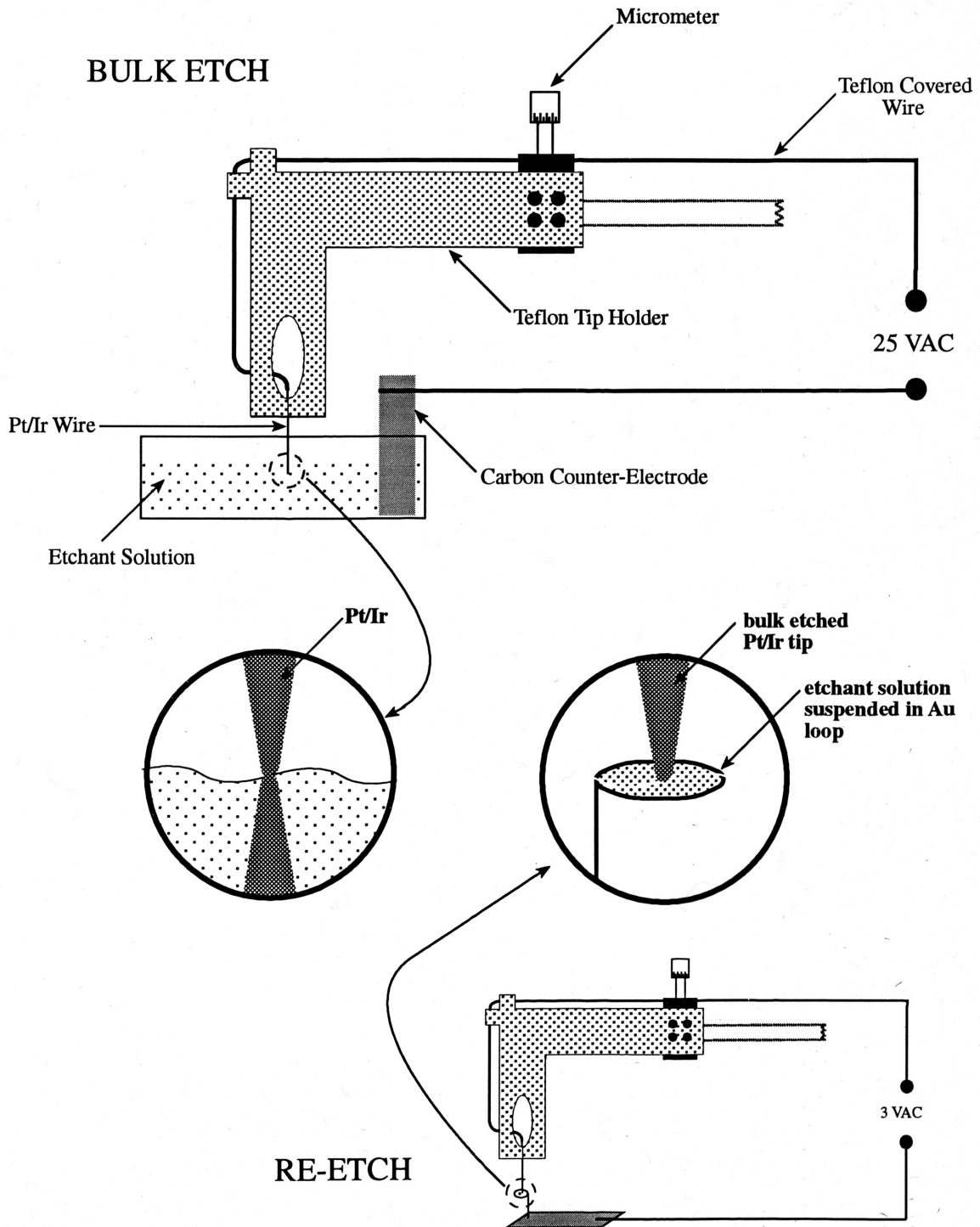ESEM Micrograph of Electrochemically Etched W Tip

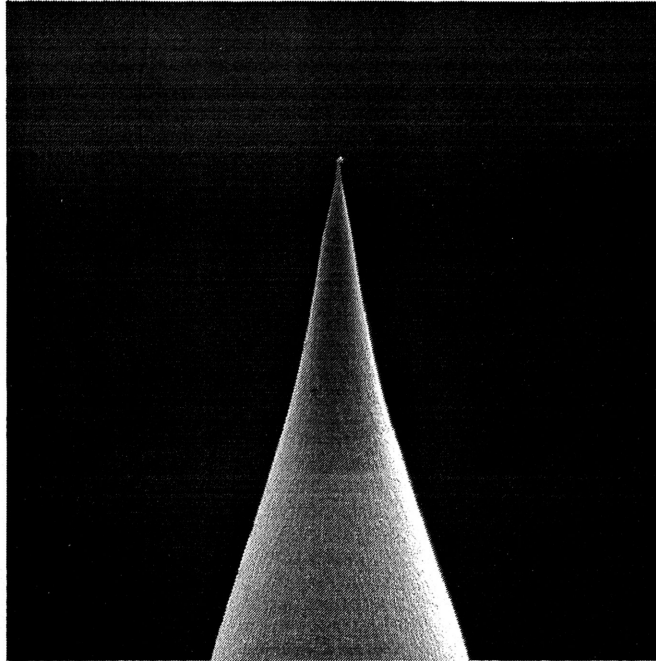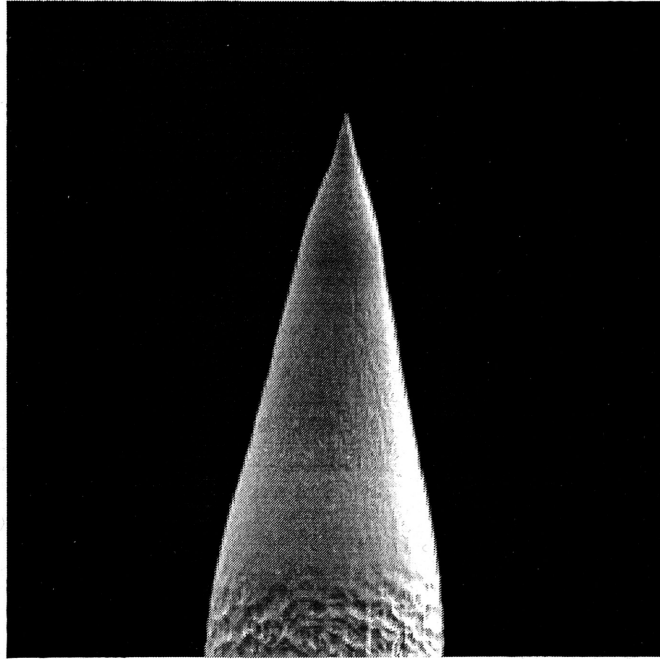Magnification: x175

——————— 100 microns

Magnification: x13500

——————— 1 micron

Figure 4
ESEM Micrographs of Mechanically Sheared Pt Tip

BULK ETCH

Micrometer

Teflon Covered Wire

Teflon Tip Holder

25 VAC

Pt/Ir Wire

Carbon Counter-Electrode

Etchant Solution

Pt/Ir

bulk etched Pt/Ir tip

etchant solution suspended in Au loop

RE-ETCH

3 VAC

Figure 5
Tip Etching Apparatus

Magnification: x175

——— 100 microns

Magnification: x5100
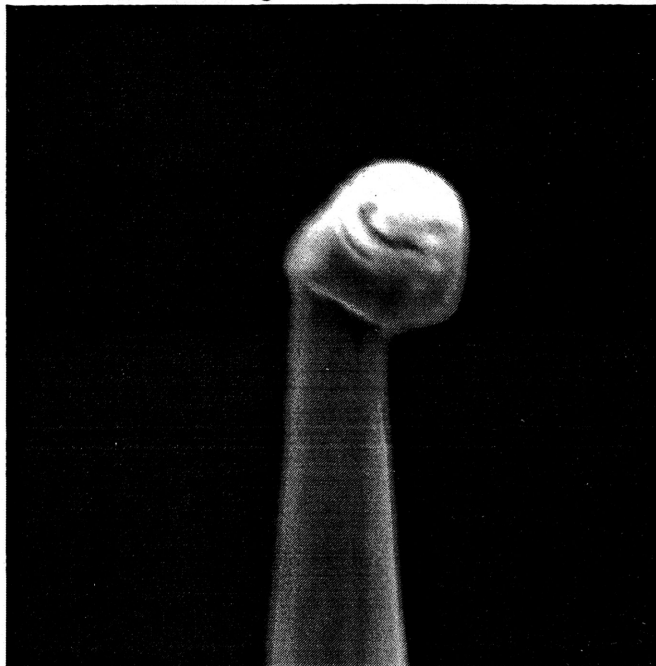
——— 2 microns

Figure 6
ESEM Micrographs of Bulk Etched
Pt/Ir Tip with Unfavorable Geometry

Magnification: x175
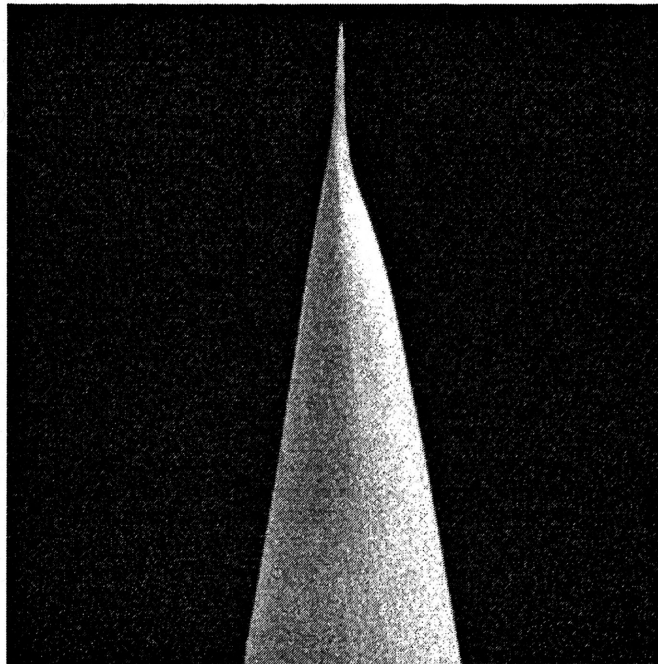
———— 100 microns

Figure 7
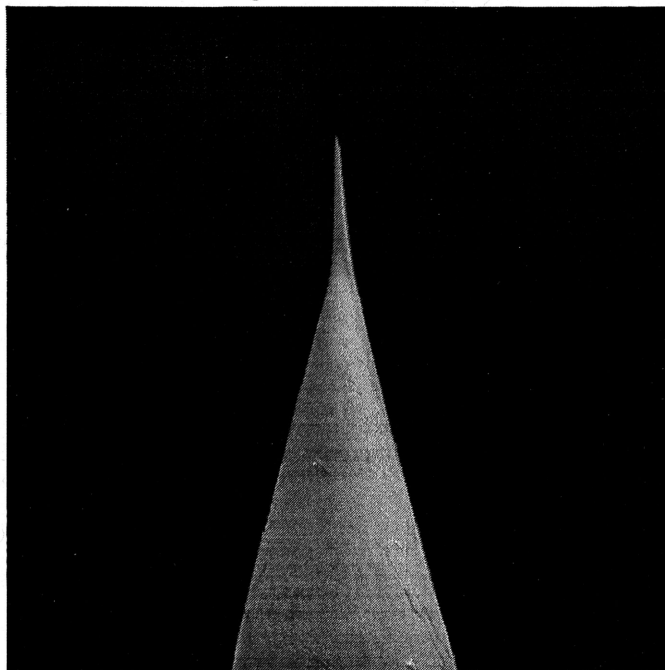ESEM Micrograph of Asymmetric Etched Pt/Ir Tip

Magnification: x175
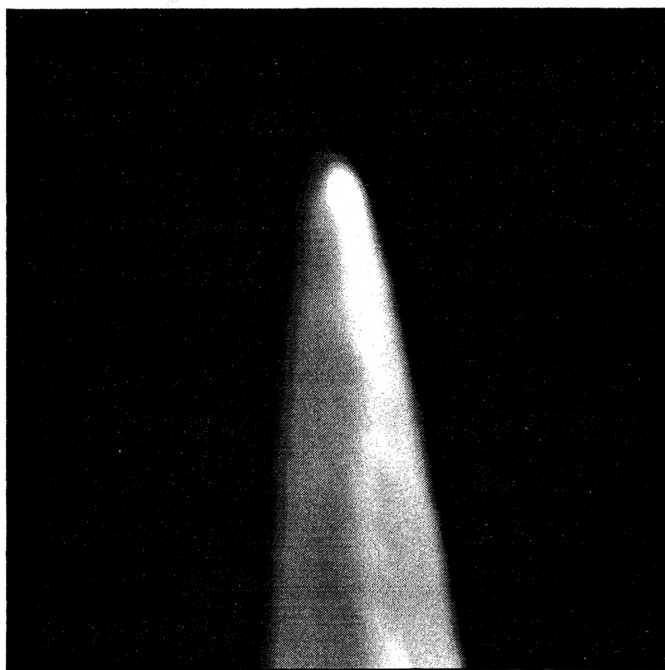

——————— 100 microns

Magnification: x13500
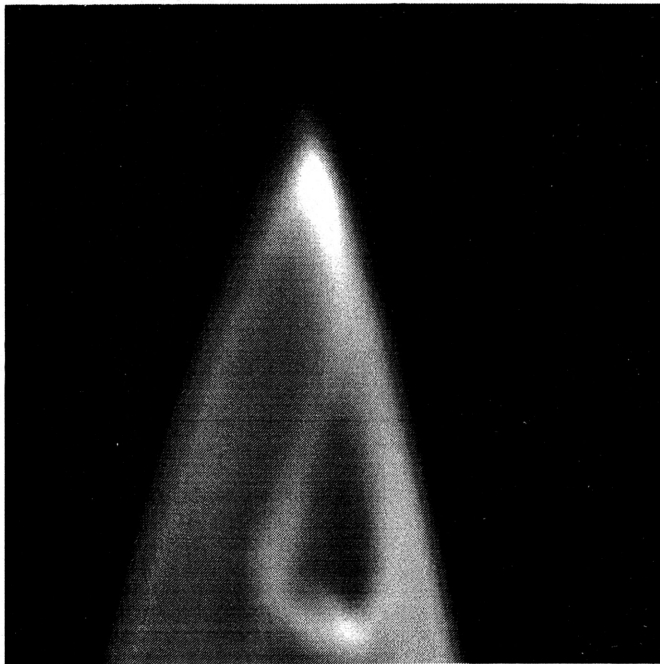
——————— 1 micron

Figure 8
ESEM Micrographs of Succesfully
Bulk Etched Pt/Ir Tip

Magnification: x175

————— 100 microns

Magnification: x13500

————— 1 micron

Figure 9
ESEM Micrographs of Succesfully
Re-Etched Pt/Ir Tip

CHAPTER 3

GaSb Substrates

In preparation for work with the Sb/GaSb superlattices, our initial experiments were performed on GaSb substrates. These experiments provided a chance to test the suitability of the new Pt/Ir tips for imaging, edge-finding, and spectroscopy. Also, the substrate material served as a good control experiment for the superlattices by providing a basis for any observations that would be made of the thin epitaxial GaSb layers in these superlattices. Analysis was performed using two re-etched Pt/Ir tips to characterize three cleaved p-type GaSb samples. The substrate material was provided by colleagues at the University of Houston.

Once the first Pt/Ir tip was loaded into the STM and observed under the stereoscopic microscope, it was obvious that the sharpness of the tips would make them difficult to observe optically. Therefore, special care had to be taken during coarse approach to ensure that they were not crashed into the samples. These Pt/Ir tips proved very capable of providing atomic resolution images of the GaSb substrate. For example, Figure 1 shows a 128 Å x 128 Å composite of the GaSb surface obtained with a tunneling current of 0.07 nA and an alternating sample bias of ± 2 V. This alternate biasing condition allows separate imaging of the anion and cation sublattices which are then combined on the computer to form the composite shown here. The atoms in the image appear as round balls arranged in rows across the surface. The Ga atoms are the dark balls and the Sb atoms are the light ones.

Prior to obtaining the clean atomic resolution image in Figure 1, images obtained with the Pt/Ir contained noise spikes. Figure 2 shows an example of this effect. The figure is a 128 Å x 128 Å image of the GaSb substrate obtained at a tunneling current of 0.07 nA and a bias voltage of +2 V. The scan direction of this figure is rotated -90° relative to Figure 1. The bias polarity denotes tunneling into the sample, which implies that Ga atoms were imaged. The small white dots and lines scattered randomly throughout the figure are the noise spikes. These spikes, which were associated with an intermittent tunneling current between the tip and sample, were attributed

to carbon contamination on the end of the tip. This carbon was linked to carbon dioxide dissolved in the de-ionized water used in the etchant solution [1]. Tip etching was later carried out using de-ionized water that had been boiled and cooled to remove the dissolved CO_2. Images, such as Figure 1, that were obtained with tips that had been etched in a solution containing the boiled de-ionized water had far fewer noise spikes. The obvious reduction in noise seen in the images provided assurance that the tips now had less carbon contamination.

Along with the regular periodic array of surface atoms, point and extended defects, such as vacancies and steps were also observed. A step is distinguished by a bright line through the image that denotes the transition between atomically flat terraces of two different heights on the surface. An example of a monatomic step on GaSb is presented in Figure 3, where a three dimensional rendering has been added to further highlight the step structure. The scan range is again 128 Å x 128 Å obtained with the same tunneling current and bias voltage as in Figure 2, but with opposite polarity. This means that tunneling occurred out of the sample and that Sb atoms were imaged.

Edge-finding on the GaSb substrate was carried out using the technique described earlier. Previous edge-finding attempts with cut Pt tips were a time-consuming task, since the operator was never certain what role the tip geometry played in the observed topography. However, with the etched Pt/Ir tips the process became routine, since the drop-off in the height of the tip as it went over the wafer edge was quite dramatic and unmistakable. Several edge images were rendered in three dimensions to give a better idea of how abruptly this transition was represented. A typical example is found in Figure 4, which shows a 2000 Å x 2000 Å region near the intersection of growth and cleavage surfaces scanned with a tunneling current of 0.07 nA and a bias voltage of -2 V.

The electronic structure of the GaSb substrate was also probed by tunneling spectroscopy. Typical spectroscopy data obtained on the substrate is shown in Figure 5, with the averaged I vs. V curve shown in the top half of the image and the log |I| vs. V curve shown in the bottom half of the image. The labels C,V, and D refer to conduction, valence, and dopant respectively. The I vs. V curve was taken as the average of 576 spectroscopy measurements taken over a 25 Å x 25 Å

scan frame at a constant tip sample separation and has the shape one would expect for a semiconductor. The portion of the curve registering a negative current signifies tunneling out of the sample valence band and into the tip. This current rises to zero in the band gap and then turns positive as the bottom of the sample conduction band is reached. Although this type of plot does well to illustrate the semiconducting properties of the GaSb substrate, it does not allow for an accurate determination of the band edge locations or for the location of the Fermi level relative to the band edges. Since the current should go to zero at the band edges, it is more appropriate to plot the logarithm of |I| vs. V. As the current goes to zero the slope of the logarithm will go to infinity, clearly defining the location of the band edge. To increase the dynamic range of the spectroscopy measurement, a second set of data points is taken within the gap with the tip closer to the sample to amplify the current. This data is then renormalized back to the previous separation distance and plotted as the open circles in Figure 5.

The standard value for the bulk band gap of GaSb is 0.75 eV and is labeled E_g in Figure 5. The experimental band gap value was determined by taking the gap to be between an extrapolation of the C region of the data to the lowest current value of the V region. This compares well with the standard value of 0.75 eV. However, other features of the spectrum do not agree as well with what was expected. The position of the Fermi level was calculated theoretically using a computer program written in preparation for these experiments. Based on the sample doping concentration of 1.0×10^{17} cm^{-3} obtained from bulk resistivity measurements, these calculations predicted that the Fermi level should lie 136 meV above the valence band. However, the data shown in Figure 5 indicate that the Fermi level is much closer than this. Another anomalous result is the large number of data points obtained within the region marked E_g, the D region of figure 5. This indicates that tunneling occurred in the gap region, and since the bias voltage was positive, current was flowing from the tip into the sample. Naively, however, there should have been no empty states open for tunneling in the gap region. These anomalies indicate that perhaps there are dopant-induced states in the gap region similar to what is observed on GaAs. Figure 6 contains the previous spectroscopy curve and an illustration of how the band diagram of the GaSb would appear with
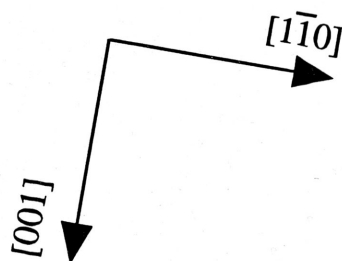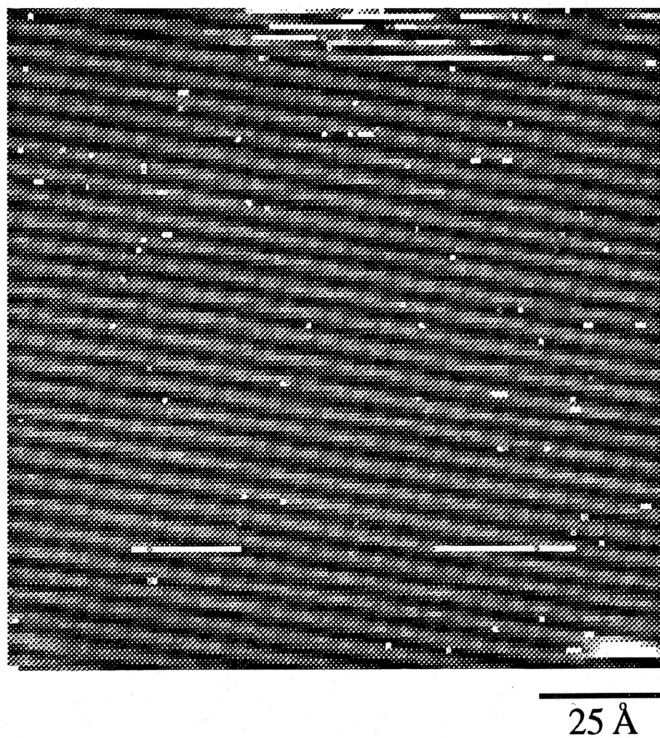
dopant-induced states present. As one can see, with the dopant induced states included, it is now plausible that tunneling could occur in the gap region explaining the spectroscopy results that were obtained.
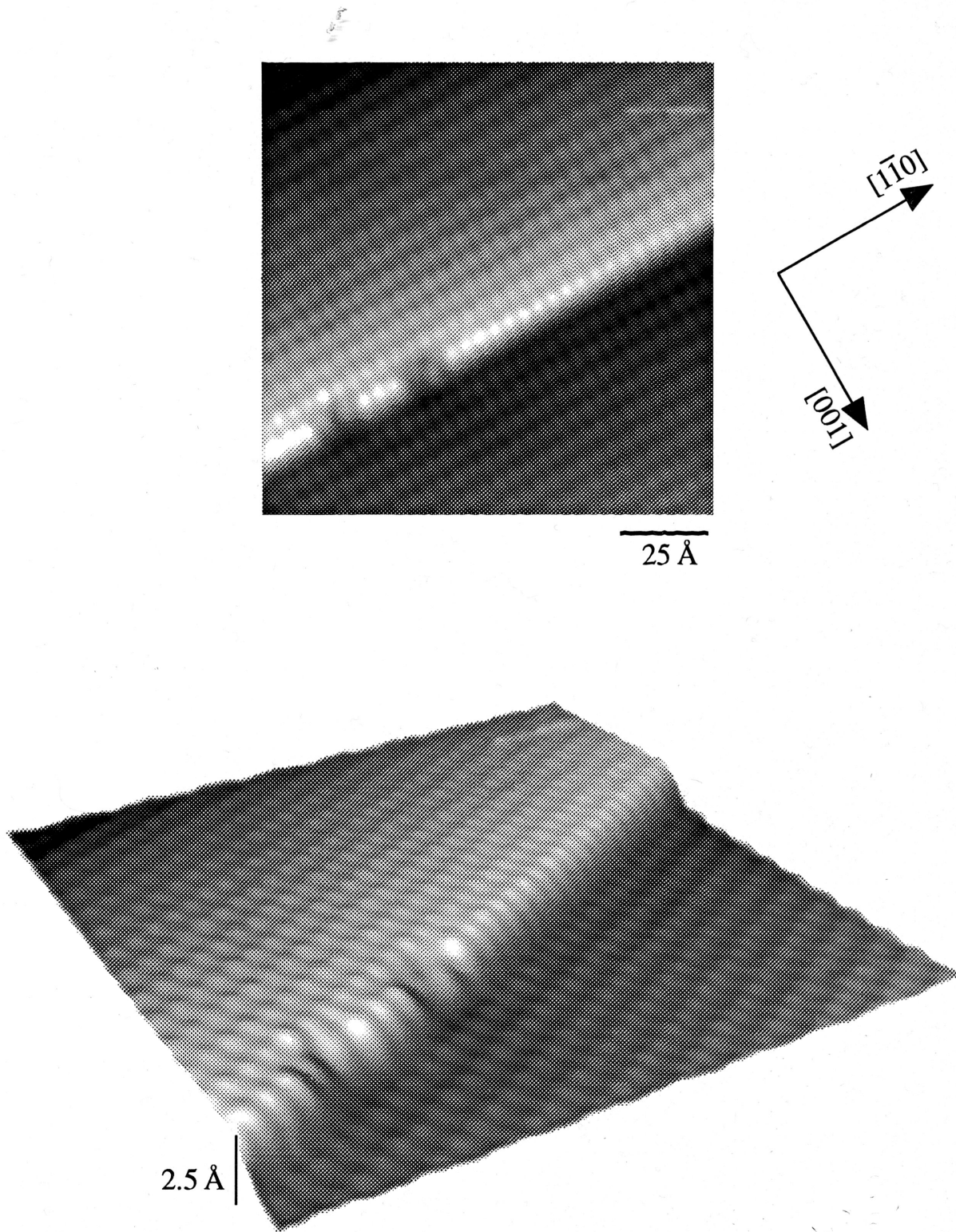
REFERENCES

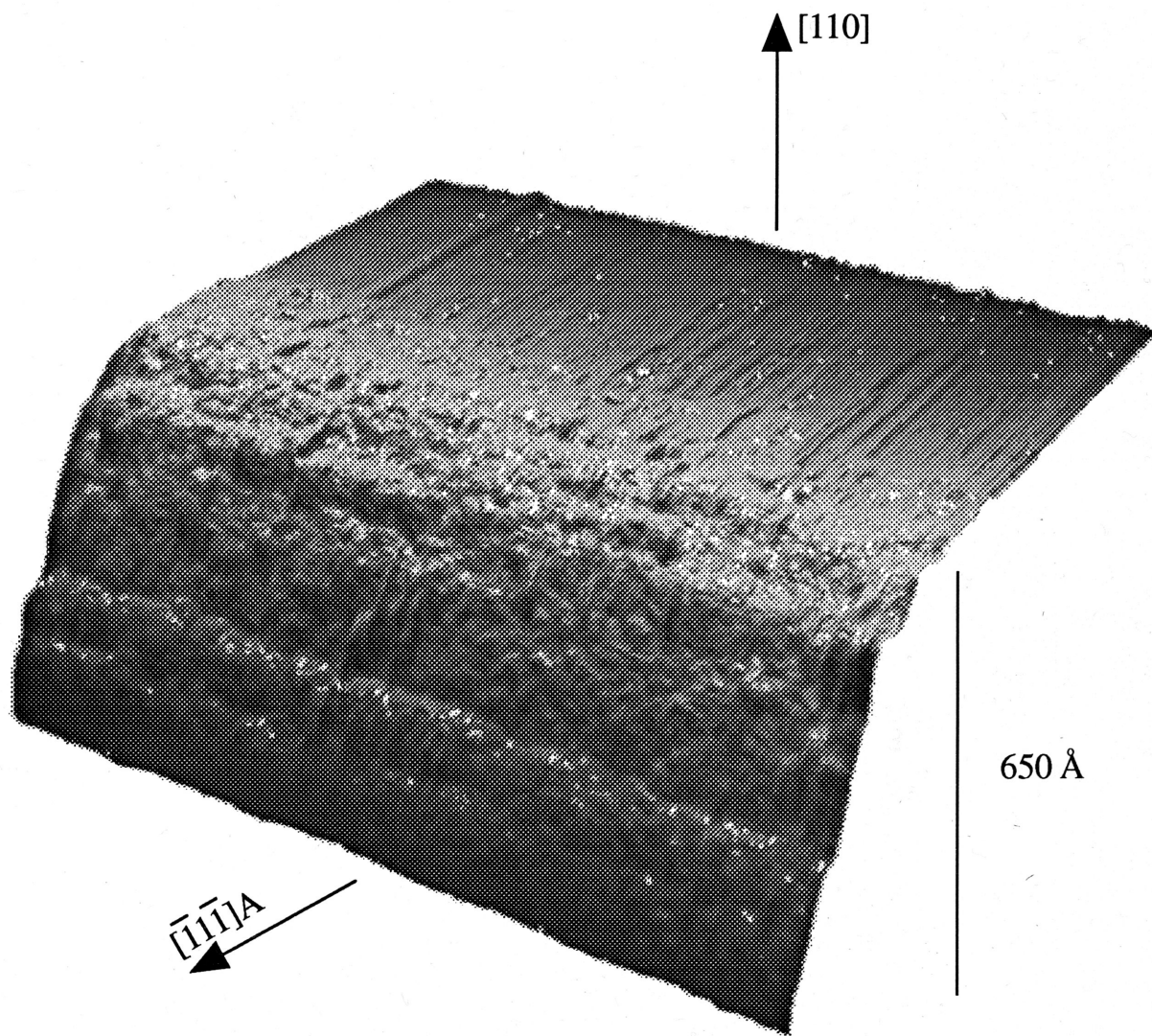[1]   I.H. Musselman and P.E. Russell, J. Vac. Sci. Technol. A **8**, 3558 (1990).
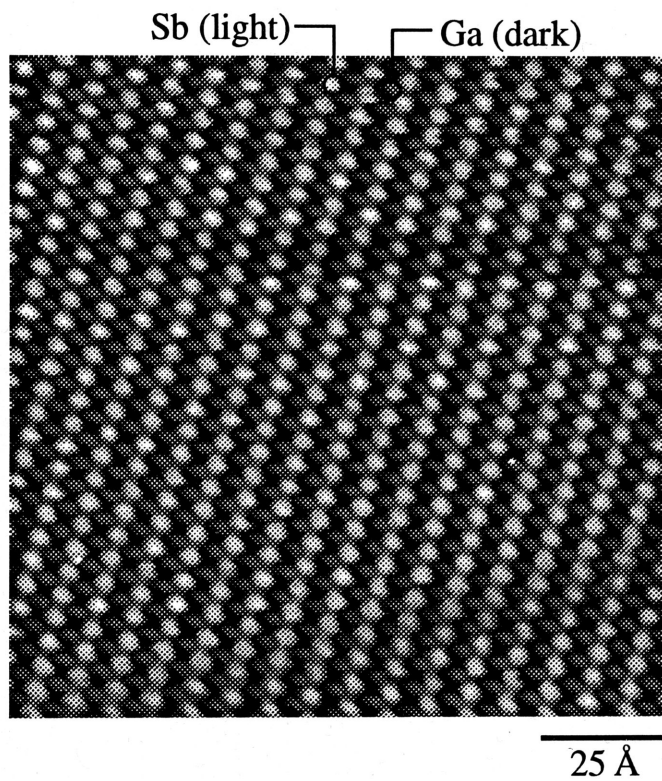
Figure 1
Clean Surface Composite Image of GaSb(110)

25 Å

[1$\bar{1}$0]

[001]

Figure 2
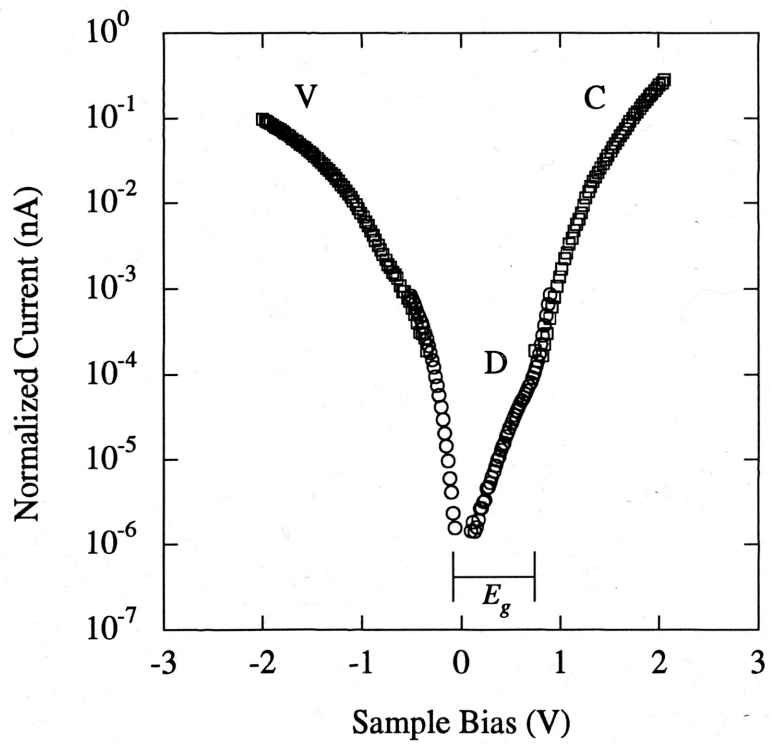STM Image of GaSb(110) Showing Noise Spikes
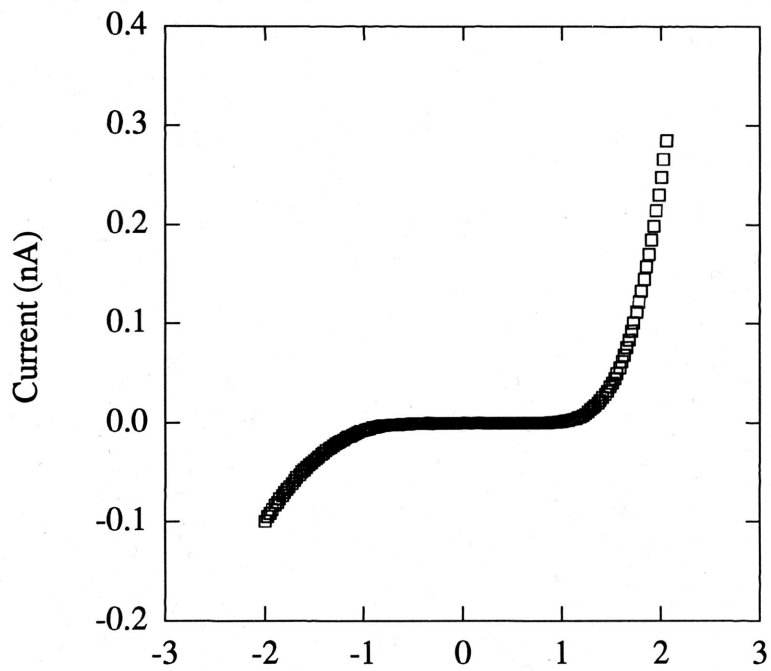
[1$\bar{1}$0]

[001]

25 Å

2.5 Å

Figure 3
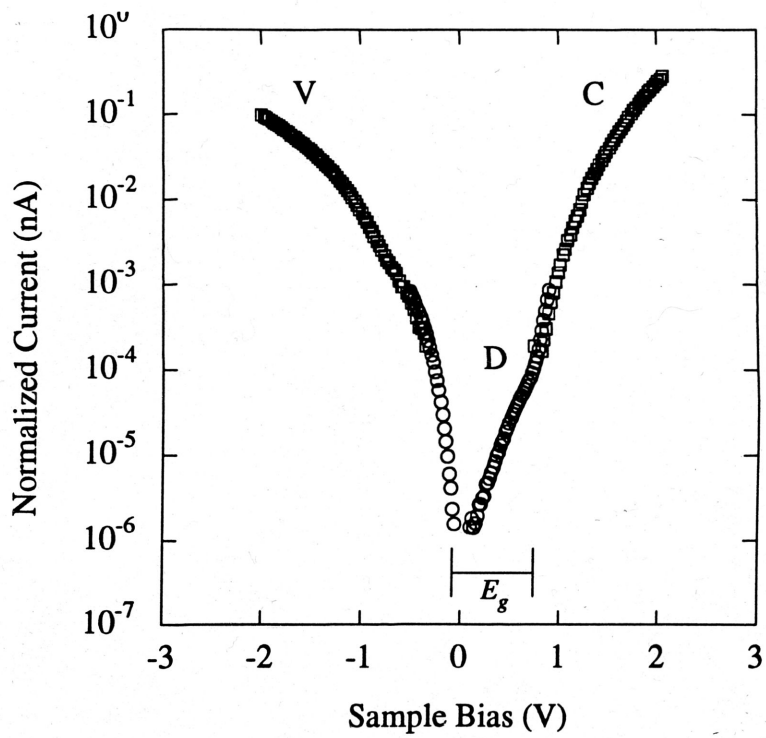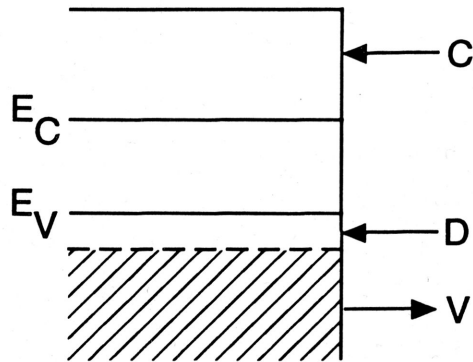2-D and 3-D STM Images of a Monatomic Step on GaSb(110)

Figure 4
3-D Rendering of the Edge of a GaSb(110) Wafer
Where Cleavage and Growth Surfaces Meet

Figure 5
Scanning Tunneling Spectroscopy of GaSb (110)

Figure 6
Band Diagram and GaSb(110) Spectroscopy Showing the Effect of Dopant-
Induced States

CHAPTER 4

Sb/GaSb Superlattices

Samples

The Sb/GaSb superlattices in this experiment were grown by molecular beam epitaxy at the University of Houston [1]. Samples were drawn from two different Sb/GaSb superlattices. The first Sb/GaSb superlattice had 37 periods of 60 Å Sb/20Å GaSb grown on a *p*-type GaSb substrate. The second Sb/GaSb superlattice had 4 periods of 1000 Å Sb/1000 Å GaSb grown on a *p*-type GaSb substrate with a 0.5 micron cap and buffer layer.

Results

Six GaSb/Sb samples were loaded into the UHV chamber for characterization. Precaution was taken when loading the samples to eliminate the possibility of Sb sublimation under the high bakeout temperatures. Bakeout involves heating up and pumping out the sections of the entry chamber where new samples are introduced. Since the high temperatures of bakeout could have damaged the samples, they were not baked before being introduced into the main chamber. This is the common procedure for all other samples to reduce outgassing. Each sample was cleaved *in situ* for characterization with the STM. Data was obtained only from four of the six samples because two of the superlattice samples shattered upon cleaving.

Before the first superlattice sample was loaded into the STM for characterization, the tip to be used was tested by imaging a GaSb substrate sample. This insured that an appropriate tip was selected to image the superlattice.

Sample 1 (37 periods of 60 Å Sb/20 Å GaSb):

After cleaving, the surface of this sample was observed under the stereoscopic microscope mounted above the STM. This examination indicated that the sample had cleaved badly, leaving a rough and jagged surface. Using the STM, the edge of the sample was found, and the tip was

moved across the sample to find the epitaxially grown layers. As this search was conducted, it became obvious that there was a large bump near the edge. By using the z-piezo to get a relative measure of the heights of surface features, the bump was measured to be approximately 2500 Å high. The bump occupied the region near the edge where the superlattice should have been observed. Images obtained of the surface were indicative of the roughness normally observed on a bad cleave. Atomic resolution images were unobtainable and the epitaxially grown layers were never found.

Sample 2 (4 periods of 1000 Å Sb/1000 Å GaSb)

Observation of this sample under the stereoscopic microscope indicated another poor cleave. After locating the edge and moving across the sample, it was apparent that a bump was located in the same position as the one observed in the first sample. Using the z-piezo readings, the surface contour was mapped out. The bump was measured to be approximately 500 Å high and extended approximately 6000 Å in from the edge before leveling off to flat substrate material. Figure 1 illustrates the measured surface contour. The figure also shows a three dimensional rendering made from an image taken on top of the bump. This 512 Å x 512 Å image was obtained at a tunneling current of 0.1 nA and a bias voltage of +2 V. The size of the features seen on top of the bump was surprisingly large and ranged up to a maximum height of 70 Å. Although images were obtained of atomic rows on the flat substrate and near the edge, it was still apparent that there was a cleaving problem, and the epitaxially grown layers were again not seen.

Sample 3 (4 periods of 1000 Å Sb/1000 Å GaSb)

The initial observations of this sample under the stereoscope indicated that the cleave had been successful, and a smooth surface was observed. However, as the contour in Figure 2 illustrates, the good cleave occurred only on the GaSb substrate, and a bump similar to that seen on samples 1 and 2 was found near the edge. The bump extended approximately 5000 Å in from the edge before the surface leveled off into the smooth GaSb substrate. Figure 2 also contains a three

dimensional rendering of a 2000 Å x 2000 Å image taken at a tunneling current of 0.07 nA with a sample bias of +2 V. This image is an example of the transition from the smooth surface onto the bump. The transition is quite dramatic as the bump was measured to be approximately 700 Å above the flat substrate. Images taken over the substrate material showed that it was possible to resolve the atomic rows. Also, the low step densities and small feature size seen on the substrate validated that the substrate cleave had been successful; however, none of the epitaxially grown layers, which should have been located in the bump region, were identified.

Sample 4 (4 periods of 1000 Å Sb/1000 Å GaSb)

This sample also gave indications of a successful cleave. Once the edge of the sample was found and the tip was moved onto the sample, it became apparent that the region near the edge had cleaved differently than previous samples. Instead of finding a bump on the edge, a jagged dip was observed. The dip extended approximately 6000 Å in from the edge. Beyond the jagged region was a smooth, atomically flat region of GaSb.

The success of this cleave compared with the previous three samples allowed for a more ambitious search for the epitaxially grown layers. Spectroscopy was performed to determine whether the semi-metallic character of the Sb layers could be observed. All spectroscopy curves had semiconductor character indicating the presence of only GaSb. A distinct contrast in the images might have indicated the transition from the GaSb to the Sb, but no contrast was ever observed. Also, no difference in the atomic crystal structure was observed, which would have been indicative of an interface between the GaSb and Sb layers.

ESEM

Following the STM experiments, ESEM images were taken of the cleaved surfaces of samples 1 and 2 to further verify that bad cleaves had been obtained. Figure 3 contains ESEM micrographs of sample 1. The cleavage face can be seen in the top image taken at a magnification of 175x. It appears as the light region in the middle of the image, running from the lower right to the upper left. The darker region in the lower right portion of the cleavage face is the side of a

bump or ridge on the surface. The lower image is a magnified view of this ridge. Large steps are visible near the edge. The appearance of this ridge and the large jagged steps verifies the observations made with the STM. Figure 4 contains ESEM micrographs of sample 3. Running from top to bottom in the upper image is the cleavage face. The cleave was perfect except for the tiny ridge seen on the left half of the face. The lower image, taken at a higher magnification, shows a narrow white line in the middle of the image on the edge of the cleavage face. This white line is a jagged ridge which corresponds with what was seen in the STM. The ridge could represent a portion of the epitaxially grown layers, or it could represent substrate material near the layers.

REFERENCES

[1]   J.A. Dura, A. Vigliante, T.D. Golding, and S.C. Moss, J. Appl. Phys. **77**, 21 (1995).

70 Å

Edge

500 Å

7000 Å

[110]

[Ī1Ī]A
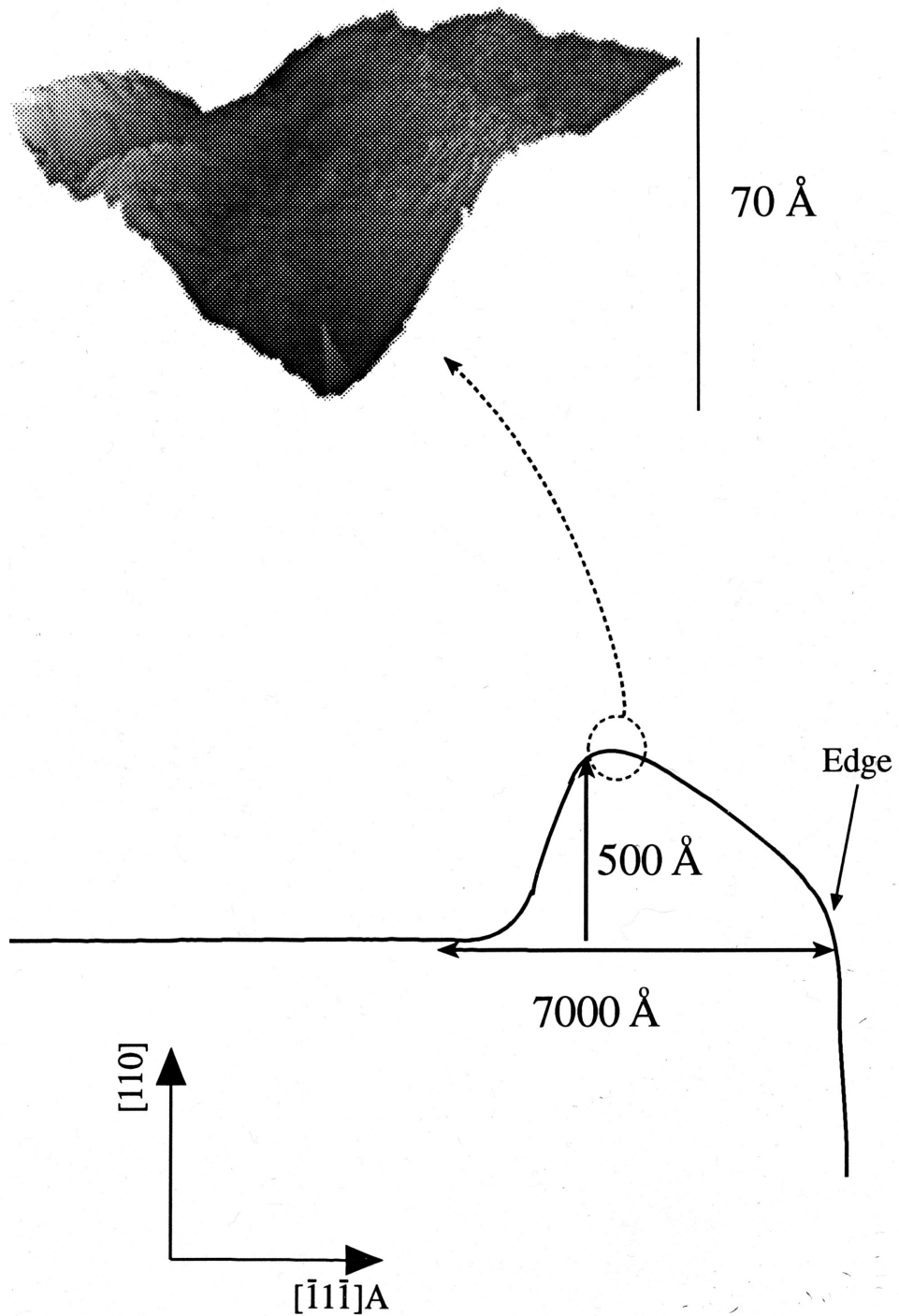
Figure 1
Surface Contour and Three Dimensional Rendering of Bump
on Sb/GaSb Superlattice Sample 2

650 Å

700 Å

5000 Å

Edge

[110]

[Ī11Ī]A
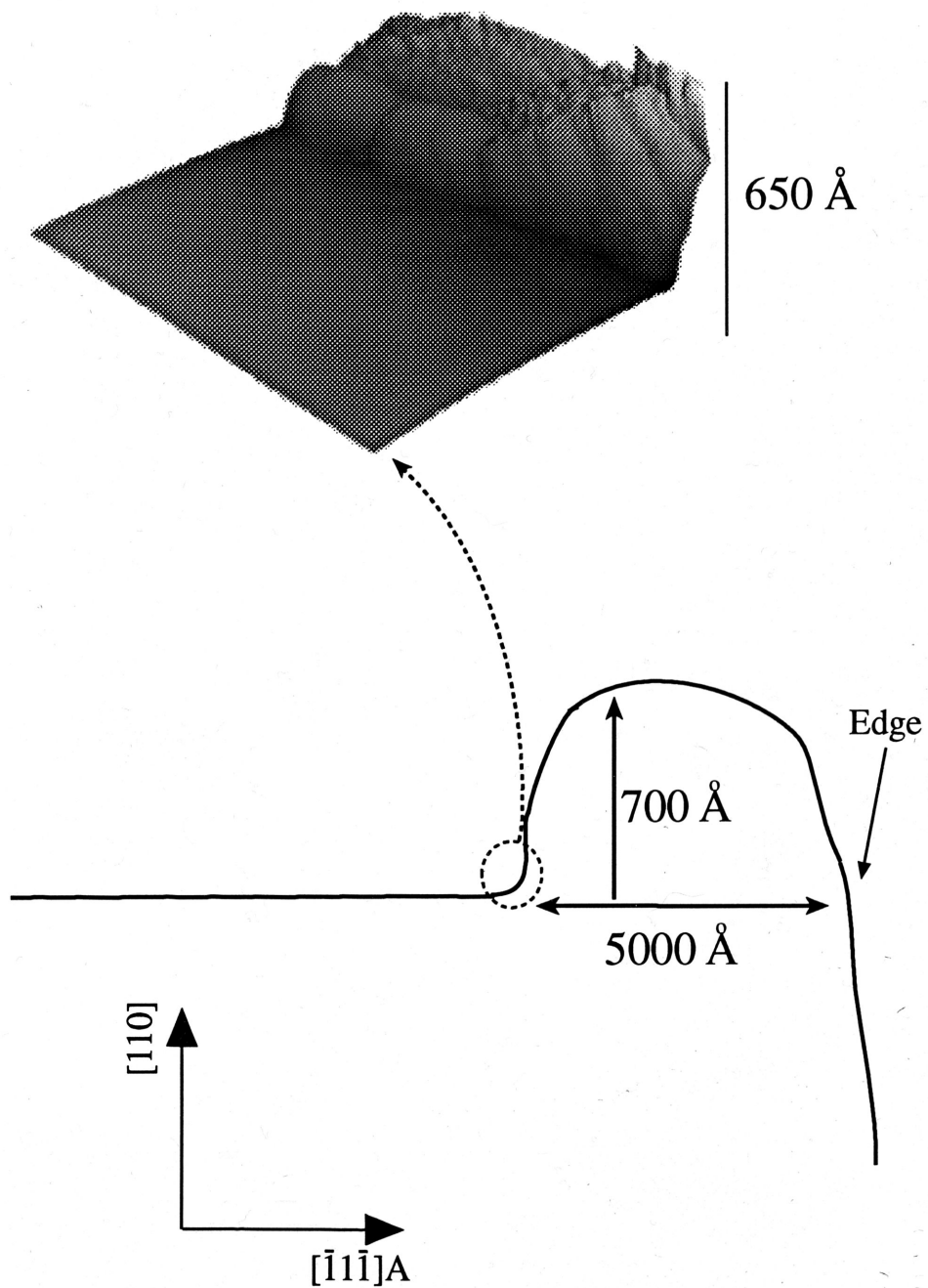
Figure 2
Surface Contour of Bump and 3-D Rendering of Transition
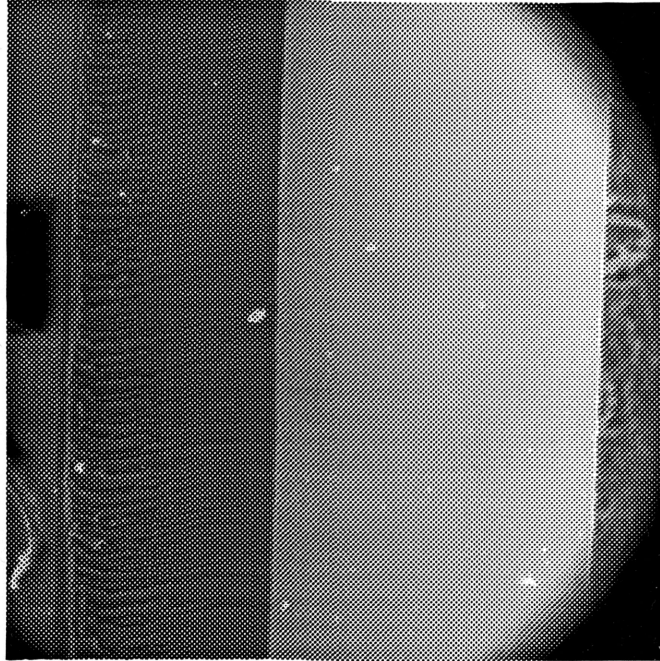from Smooth Surface to Bump on Sb/GaSb Superlattice Sample 3

Magnification: x175
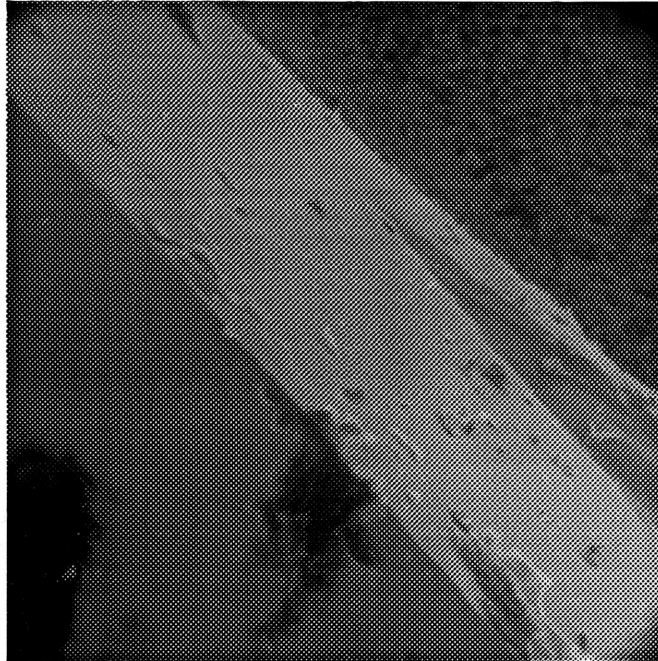
——————— 100 microns
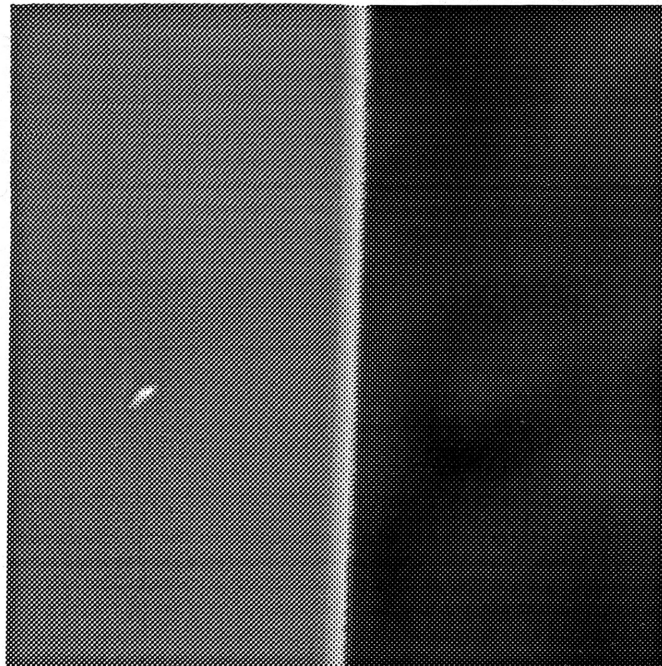
Magnification: x1200

—————— 10 microns

Figure 3
ESEM Micrographs of the Cleaved Surface of
an Sb/GaSb Superlattice Sample 1

Magnification: x175

——— 100 microns

Magnification: x2200

——— 5 microns

Figure 4
ESEM Micrographs of the Cleaved Surface of
an Sb/GaSb Superlattice Sample 3

CHAPTER 5

Conclusions

The tip characterization work demonstrated that it was possible to reproducibly fabricate sharp STM tips by electrochemically etching Pt/Ir (80:20) in a saturated solution of $CaCl_2/H_2O/HCl$ using boiled (de-ionized) water to reduce carbon contamination. It is now possible to quickly bulk etch and re-etch tips, determine their suitability under the optical microscope, and recover tips with unfavorable geometries. These tips can be used to obtain atomic resolution images, perform tunneling spectroscopy, and quickly locate the edge of a cleaved sample.

Tunneling spectra from GaSb substrates showed surprising features. The value obtained for the surface Fermi level differed from that calculated based on transport measurements of the free carrier concentration. There was also a measurable tunneling current within the voltage region corresponding to the bulk band gap. The origin of both of these observations is not yet definitively established, and must be addressed by further experiments.

Experiments on the Sb/GaSb superlattices were hampered by a consistent cleaving problem. All of the superlattice samples retained some roughness near the edge following cleavage, and in all cases the epitaxially grown layers were never found. This suggests that the epitaxial layers were ripped off during cleavage. The problem may be linked to differing growth temperatures for the buffer layer and superlattice structure. New structures are now being grown at the University of Houston to investigate whether the cleavage difficulties are indeed growth temperature dependent, and to determine which layer is introducing the problem. First, a sample with just the GaSb buffer layer will be grown and then cleaved for observation with the STM. If this structure cleaves properly, a second sample will be constructed with a layer of GaSb grown on top of the buffer layer at the superlattice growth temperature. If this sample also cleaves properly, a third sample will be grown in which a layer of Sb is introduced between the two layers of GaSb.

These successive steps should identify the source of the cleavage problem so that we can fabricate heterostructures which may be successfully characterized with the STM.